Manuscript received .....

Affiliation of author:

Prof. José Manuel Gutiérrez

Dept. of Applied Mathematics

E.T.S.I. Caminos

Universidad de Cantabria

Santander (39005) Spain

email: manuel.gutierrez@unican.es

Controlling and Exploring Nonlinear Dynamics in Circuits by Sporadic Proportional Pulses

P. Ruiz, J.M. Gutiérrez, and J. Güémez

Pablo Ruiz is a fellow at the Insituto de Física de Cantabria, CSIC-Universidad de Cantabria, Spain.

J.M. Gutiérrez is with the Department of Applied Mathematics and Computational Sciences, University of Cantabria, Spain. E-mail: gutierjm@unican.es.

Julio Güémez is with the Deparment of Applied Physics, Universidad de Cantabria, Spain

Abstract

We present some experimental evidence of control and anticontrol of chaos in chaotic circuits using a simple impulsive method which does not require any knowledge about the systems dynamics. The method works by introducing instantaneous pulses in some system variables –in this paper the pulses are applied to a capacitor voltage– and, hence, does not modify the system itself. When varying the control parameters (amplitude and frequency of pulses) we obtain a bifurcation structure similar to the one obtained when varying some system parameters. Therefore, this controller allows us investigating the dynamics of a given circuit and provide us a versatile device for performing both control or anticontrol. In particular we show how a double-scroll chaotic system is stabilized in period three, single-scroll, period-4, period-2, period-1, fixed point, following a inverse bifurcation route as a function of the pulses amplitude (chaos control). It is also shown how a periodic Chua's circuit is driven to chaotic behavior (chaos anticontrol).

Keywords

Chaos control, anticontrol.

I. Introduction

One of the most surprising, and recent, applications of chaos theory is the possibility of switching the dynamics of nonlinear systems from chaos to order (chaos control), or reversely from order to chaos (chaos anticontrol) [1]. This versatility of nonlinear systems lies in the fact that chaotic motion includes an infinite number of embedded unstable periodic orbits, that can be stabilized by appropriate mechanisms. This possibility gives a new meaning to nonlinear systems, since they can be seen now as an unlimited reservoir of different behaviors to be tuned on or off using simple mechanisms. The first chaos control algorithm was the celebrated OGY method [2], able to stabilize unstable periodic orbits containing a saddle node point using appropriate parameter perturbations; the method was later modified for inducing chaos in periodic systems [3]. Since then, many different approaches have been proposed for chaos control and anticontrol, including stochastic and periodic system perturbations [4], [5], noise addition [6], [7], feedback continuous procedures [8], [9], etc. (see [10] and references therein for a detailed description).

Although these methods were initially developed for computational applications [11], most of them have been implemented in practical systems. The first experimental evidence of chaos control was found using the OGY method to control the chaotic vibrations of a magnetoelastic ribbon [12]. This method and some variations have also been used to control a diode resonator circuit [13], a parametrically driven pendulum [14], the bursting behavior of a neuronal population [15], or solid-state lasers [16]. In all cases, the control is achieved by manipulating an accessible system parameter and requires some knowledge of the model equations, or a previous study of the system dynamics.

Recently, a new chaos suppression method which acts on the system variables has been introduced [17], [18]. This method does not require any knowledge about the model equations or the system dynamics and it is, therefore, a convenient method for practical settings. In this paper, we present an electronic implementation of this algorithm and its application both for chaos control and anticontrol. For instance, we show how this simple method can be easily applied to a Chua's double-scroll circuit, driving it to

several periodic regimes following a period-doubling bifurcation route. We also illustrate the opposite situation where a periodic Chua's circuit is forced to exhibit chaotic behavior. Furthermore, we present an application of the control device for exploring the dynamics of nonlinear circuits, discovering those behaviors embedded in their nonlinear structure (periodic and chaotic regimes, bifurcation structure, etc.). Note that this is done with no manipulation of the original system parameters.

In Sec. II we describe the cubic Chua's circuit to be used to illustrate the proposed methodology; the evolution equations are presented and the corresponding adimensional set of differential equations, more simple to be numerically integrated by computer, is derived. In Sec. III we describe the original method and a new implementation, more accurate for experimental and numerical comparison. Then, the electronic control and anticontrol device is described in detail. In Sec IV experimental results are presented and compared with numerical results obtained from the adimensional system. Finally, a brief summary and some additional notes about the method and its possibilities are presented in Sec. V.

II. The Chua's cubic chaotic circuit

Analog electronic circuits are well-known examples of systems exhibiting chaotic behavior. Among these systems, the Chua's circuit [19] has become a paradigm for experimental applications, due to its simplicity and richness of behaviors [20]. Chaos synchronization and control, and efficient experimental transmission of information, have been reported using this circuit.

The Chua's circuit is a simple autonomous circuit with an inductor, two capacitors, a resistor and a single nonlinear resistor. In the original paper, the nonlinear resistor used has a three-segment piecewise-linear $v-i$ characteristic, although this nonlinear characteristic can also be a smooth polynomial. In this paper we use the cubic Chua's circuit with a cubic nonlinearity [21], also known as Van der Pol-Duffing oscillator [22] (see Fig. 1). The following set of differential equations are obtained by applying Kirchhoff's laws to the schematic of the circuit shown in Fig. 1(a):

$$\begin{aligned} C_1\frac{\mathrm{d}v_1}{\mathrm{d}t} &= \frac{1}{R}\left(v_2-v_1\right)-I(v_1), \\ C_2\frac{\mathrm{d}v_2}{\mathrm{d}t} &= \frac{1}{R}\left(v_1-v_2\right)+i_{\mathrm{L}},\ \frac{\mathrm{d}i_{\mathrm{L}}}{\mathrm{d}t}=-\frac{1}{L}\left(v_2+R_{\mathrm{L}}i_{\mathrm{L}}\right), \end{aligned} \tag{1}$$

where $I(v_1)$ represents the cubic nonlinear resistor with $v-i$ characteristic $I(v_1)=Av_1+Bv_1^3$ (see Fig. 1(b)).

We constructed this circuit with the following values: $R=3300\ \Omega$ and $R_{\mathrm{L}}=20\ \Omega$; $C_1=1.2$ nF, $C_2=12$ nF, $L=10$ mH and $A=-3.3\times10^{-4}$ AV^{-1} (or S), $B=1\times10^{-6}$ AV^{-3} (or SV^{-2}). For the cubic element we used a set of analog multipliers (AD633) and operational amplifiers (TL084 or equivalent) as shown in Fig. 1(a) (see [23] for additional implementation details); the variable resistor $R10$ is included in the circuit to control the cubic coefficient and vary the magnitude of the attractor. With this implementation the Chua's circuit can also be seen as a physical realization of the Van der Pol-Duffing oscillator [24]. The tolerances of the resistors, capacitors, and inductors used are 1%, 5% and 10%, respectively. All the

experimental results have been measured using a Tektronix TDS 724D digital oscilloscope with 2 GS/s. Analog simulations of circuit Eq. (1) are carried out with PSpiceAD program in order to test the real circuit as well as to explore parameters values with technological interest but out of our experimental possibilities.

In order to compare experimental and numerical results, an appropriately rescaling is introduced. With the corresponding change of variables ($v_1 \equiv x; v_2 \equiv y; R_{\rm L} i_{\rm L} \equiv z; \kappa \equiv t/RC_2$) one can rewrite (1) obtaining the following adimensional set of differential equations

$$\begin{aligned} \frac{{\rm d}x}{{\rm d}\kappa} &= \alpha\left[y - x - I(x)\right], \\ \frac{{\rm d}y}{{\rm d}\kappa} &= x - y + z,\ \frac{{\rm d}z}{{\rm d}\kappa} = -\beta y - \gamma z, \end{aligned} \tag{2}$$

with $I(x) = ax + bx^3$ and where κ is an adimensional time unit.

The adimensional system parameters corresponding to the above chosen values are $\alpha = C_2/C_1 = 10$, $\beta = R^2 C_2/L = 13.068$, $\gamma = RR_L C_2/L = 0.00792$, with $a = -1.089$ and $b = 0.0033$. For this set of values, the circuit exhibits a chaotic double-scroll attractor. The interval of real time and the interval of time in the adimensional system are related by $\kappa = 2.5 \times 10^4 t$ (for the numeric experiments, integrating the adimensional system, we adopt the time step $\tau = 2.5 \times 10^{-3}$, equivalent to 100 ns).

As we mentioned above, one of the main advantages of this circuit for experimental applications is the richness of behaviors. For instance, by varying α in Eq. (2) –equivalent to the capacitance C_2 in the physical implementation– with fixed values of $\beta = 13.068$ and $\gamma = 0.00792$, a period-double bifurcation diagram is obtained, from fixed point, to chaotic single scroll, and to chaotic double-scroll. Similarly, taking β as alternative bifurcation parameter, with fixed $\alpha = 10$ and $\gamma = 0.00792$ values, an inverse Feigenbaum route to chaos is observed as β increases from $\beta = 10$ to $\beta = 20$. Therefore, the richness of behaviors embedded in this nonlinear circuit manifests in the bifurcation routes obtained when varying some of the system parameters. We shall describe later in this paper how this bifurcation structure can be also uncovered and mastered connecting the circuit to a control device which does not act on the system parameters.

III. The chaos control algorithm

A. The numeric scheme

Recently, it was proposed a new method for suppressing chaos in nonlinear systems by adding sporadic proportional pulses to some system variables both in arbitrary [17] or system-related [18] time scale T. The pulses take the following form:

$$x_i(t) \leftarrow x_i(t)\left[1 + \lambda_i\, \delta\left(t - jT\right)\right],\ j = 0, 1, 2, \ldots. \tag{3}$$

where x_i represents the ith variable of the system, λ_i regulates the intensity of the perturbation applied to the ith variable, and δ represents the Dirac's δ function. From a numerical point of view this method

can be easily implemented using the integration step τ as an arbitrary time unit. Thus, the pulses are introduced after k integration steps $T = k\,\tau$ (for some k). In this paper we shall consider this simple form, since the use of system-related time scale (e.g., the return time to a Poincaré section) requires some knowledge of the system dynamics as well as implementing additional algorithms [18].

Although the algorithm in Eq. (3) dependens on two parameters T and λ (we assume that all variables have the same λ_i value or that a single variable is perturbed), it was found that similar results can be achieved using pairs of values (T, λ) and (T', λ') with $\lambda'/T' = \lambda/T$ [17]. This result indicates that the stabilized behavior achieved with control parameters λ and T can be maintained by applying stronger −or weaker− pulses, $k\,\lambda$, with larger −or shorter− period $k\,T$.

Due to the unphysical character of these instantaneous pulses, we consider a variation of this method in order to compare the numerical simulations with the experimental results presented below. To this aim, the control algorithm is not supposed to act instantaneously, but certain temporal extension is considered for the kick, where it acts linearly. When using an integration method with time step τ, the interval of time between kicks, T, is divided into $T/\tau = N$ steps, the control kick acts during the first n steps of this interval. Thus, Eq. (3) can be generalized as:

$$x_i(t) \leftarrow x_i(t) \left[1 + \frac{\lambda}{n} \sum_{k=0}^{n-1} \delta\left(t - j\,\tau\,N - k\,\tau\right) \right],\ j = 0, 1, 2, \ldots \tag{4}$$

where N and n are fixed natural numbers used by the control algorithm and the strength of pulse is λ/n. Note that with $n = 1$, the original Eq. (3) is recovered.

In the same sense that referred above for λ and T, it is possible to find a numerical relationship between the strength of pulses, λ, and the duration of sub-interval of application, n, in order to stabilize similar periodic orbits. Thus, pairs (λ, n) and (λ', n'), with $\lambda\,n = \lambda'\,n'$, produce the same stabilized dynamics (at constant T).

B. The electronic implementation

Now we briefly describe an electronic implementation of the above control scheme (see Fig. 2). At point p a continuous sample of voltage v_2 is obtained with no perturbation of the system; for this task we use buffer B. This signal is amplified by a factor χ either in the form $v_{01} = +v_2\chi$ (externally controlled by resistance $Ra2$), or $v_{02} = -v_2\chi$ (controlled by resistance $Ra5$). An external switch (s) allows choosing the $\pm$ character of the amplification. An internal switch connects the device that converts this voltage into intensity –using a voltage-intensity conversor (VIC)– at equally spaced intervals of time $t_{\rm I} \approx 20\ \mu s$. This conversor is connected during the interval of time $t_{\rm R}$. A variable intensity $i_{\rm p} = v_{0i}/R_{\rm S}$ is reinjected at point p by varying the resistance $R_{\rm S}$. The duration of this intensity pulse is $t_{\rm R} \approx 500$ ns. The increment of voltage imposed at point p is

$$\Delta v_2(C_2) \approx \frac{1}{C_2} \int_0^{t_{\rm R}} i_{\rm P} {\rm d}t \approx \frac{i_{\rm P}}{C_2} t_{\rm R} = \pm v_2 \frac{\chi}{C_2 R_{\rm S}} t_{\rm R} \tag{5}$$

and acts on capacitor C_2 by quasi-instantaneous pulses. This relationship is only valid for low $t_{\rm R}$ values. The effect of the reinjected intensity is to vary the potential, v_2, as

$$v_2 \leftarrow v_2 \pm v_2 \frac{\chi}{C_2 R_{\rm S}} t_{\rm R} = v_2 \left[1 \pm \frac{\chi t_{\rm R}}{C_2 R_{\rm S}} \right] . \tag{6}$$

By comparison with Eq. (3), it is possible to identify $(\chi t_{\rm R}/C_2 R_{\rm S}) \equiv \lambda$ as the proportional pulse strength control parameter. Then, proportional changes into variable v_2 can be introduced by choosing $\pm\chi$, $t_{\rm R}$ and $R_{\rm S}$ parameters in the control circuit. The identification of control parameters with Eq. (4) is $\chi t_{\rm R}/C_2 R_{\rm S} \equiv \lambda$, $t_{\rm I} \equiv N\,\tau$ and $t_{\rm R} \equiv n\,\tau$. Because the physical implementation, the returned signal is not instantaneous and during interval of time $t_{\rm R}$ the deposited charge over the capacitor C_2 varies linearly. Then, as more narrow the interval of time $t_{\rm R}$, more instantaneous will be the corresponding control pulse.

IV. Experimental and numerical results

Before implementing the control circuit, we performed several numeric simulations to check the performance of the modified control algorithm above presented. To this aim, the adimensional system (2) was integrated with a fourth-order Runge Kutta algorithm, considering the following parameters for the control algorithm: $\tau = 0.00025$, $N = 2000$ and $n = 10$, with $\lambda = -0.15$ in Eq. (4). After a transient time of uncontrolled motion, the controller is switched on and pulses are applied to y. Fig. 3(a) shows how the motion is quickly stabilized to a period-2 orbit.

In order to verify the above simulation, the control algorithm was implemented on the PSPiceAD analog simulator. Figure 3(c) shows the evolution of capacitor voltages v_1 and v_2 obtained in the same conditions of the previous experiment. After 5 ms of uncontrolled motion, the controller is switched on and pulses are applied to v_2; the interval of time between pulses is 20 μs and the duration of pulses is ≈ 100 ns. Figure 3(b) shows a magnification of a pulse; from this figure it can be measured a 15% proportional decrement of variable v_2 after the kick ($\lambda = -91.38/620 \approx -0.15$) in agreement with the numeric simulations.

Once the control algorithm was validated, the circuit shown in Figure 2 was built and the above experiment was also performed and measured on an oscilloscope. Figure 4(a) shows the initial double-scroll chaotic attractor of the circuit, with the above given component values. Afterwards, the control circuit is switched on −acting on switch (s) (see Fig. 2)−, introducing pulses on voltage v_2 of capacitor C_2 every $\tau = 20\mu$s; the values of the signal v_2 sampled to obtain the proportional pulses are shown in the lower panel of Figure 4(b). The upper panel shows a magnification of a pulse, where a proportional decayment on voltage v_2 can be measured with $\lambda \approx -0.15$, in agreement with the analog and numeric simulation results above presented. An oscilloscope view of the stabilized period-2 orbit is shown in Figure 4(c).

Figures 4(d) and (e) show the results obtained applying the same control, but decreasing the interval of time between pulses to $\tau' = 10\mu$s and reducing the pulses strength by the same factor ($\lambda' \approx -0.077$, see Fig. 4(d)). Figure 4(e) shows that, as we mentioned in Section III.A, the above stabilized period-2

orbit is maintained with this control settings, since $\tau/\lambda \approx \tau'/\lambda'$. The difference between Figures 4(c) and 4(e) is due to the magnitude of the pulses. To illustrate this point, the pictures were taken from the oscilloscope with 500 M samples/s, which allowed recording several pulse samples.

Apart from the above period-2 orbit, a great variety of behaviors can be obtained when considering the pulses strength as a new system parameter to be varied. Furthermore, it can be shown that the new system follows a bifurcation route similar to the one exhibited by the original system. In Fig. 5 we show a numerical comparison between the bifurcation diagram of the system Eq. (2), with α acting as a bifurcation parameter (a), and the bifurcation diagram of system (2) with $\alpha = 10$, connected to the control mechanism (6) using the pulses strength λ as bifurcation parameter (b). This result emphasizes that important information about the system dynamics can be obtained with no manipulation of the original system parameters, but using the auxiliar controller presented in this paper. Note how in the above examples, negative pulses are added into the system leading it to a more regular behavior.

We also performed the opposite experiment of inducing chaotic behavior in a periodic Chua's circuit adding positive pulses. For instance, considering a period-2 orbit and applying the control device with $\tau = 10\mu$s and $\lambda \approx 0.08$, the circuit exhibits a double-scroll attractor. Note how pulses of the same intensity, but opposite signs, allow us switching from chaos to order, or from order to chaos, a given system.

In order to illustrate the capabilities of the controller for exploring dynamics in nonlinear circuits, Figure 6 show a sequence of oscilloscope views corresponding to some of the stabilized circuit states, obtained by applying the control algorithm with decreasing λ values to the double scroll Chua's circuit shown in (a): From single-scroll (c), to period four (d), two (e) and one (f). An orbit corresponding to a periodic window near the chaotic regime is also presented in (b) to illustrate how small pulses can stabilize periodic orbits. A bifurcation diagram indicating the location of the stabilized orbits (depending on the value of the pulses strength) is also included. Thus, this control method of control is able to explore the whole bifurcation diagram for the system without changing its parameters.

Similar results have been also obtained with piece-wise nonlinearity Chua's circuit, indicating a possible generalization of the present results.

V. Summary

Implementations of chaos control have moved from purely theoretical and computational studies to experiment, proving that chaos may be exploited to perform practical functions. In this work some experimental results of chaos suppression on an electronic circuit are reported. The method works by adding proportional pulses in the system variables. In order to be more realistic and accurate with the experimental non instantaneous character of physical pulses, the original control algorithm has been modified. The physical implementation of the modified method has been corroborated with circuit analog simulations and with numerical integration methods.

The simplicity of the method gives the electronic controller a flexibility that other experimental settings

lack of. We show how the circuit dynamics can be easily switched among different chaotic and periodic states. Moreover, it is shown that the stabilized periodic motion closely resemble the unstable periodic motion embedded in the chaotic attractor. Bifurcation diagrams obtained when varying a system parameter (with no control) and a control parameter are shown to be very similar. This similarity constitutes an heuristic prove about the hypothesis that this method of control permits an exploration of the system dynamics without introducing changes in its parameters set.

VI. Acknowledgements

We acknowledge Dr. M.A. Rodríguez and Dra. A. Suárez for helpful discussions.

References

[1] G. Cheng "Chaos: control and anti-control," *IEEE Circ. Sys. Newslett.*, March 1998, pp.1-5.

[2] E. Ott, C. Grebogi, J. A. Yorke, "Controlling chaos," *Physical Review Letters*, vol. 64, pp. 1196-1199, 1990.

[3] V. In, S. Mahan, W. L. Ditto and M. L. Spano "Experimental Maintenance of Chaos," *Physical Review Letters* vol. 74, pp. 4420, 1995.

[4] R. Lima and M. Pettini, *Physical Review A*, vol. 41, pp. 726, 1990;

[5] R. Chacón and J. Díaz-Bejarano, *Physical Review Letters*, vol. 71, pp. 310, 1993.

[6] J.M. Gutiérrez, A. lglesias, and M.A. Rodríguez, "The logistic map driven by dichotomic noise," *Physical Review E*, vol. 48, pp. 2507, 1993.

[7] S. Rajasekar and M. Lakshmanan, *Physica D*, vol. 67, pp. 282, 1993.

[8] K. Pyragas, *Physics Letters A*, vol. 181, pp. 203, 1993.

[9] X.F. Wang, G. Cheng, and X. Yu Anticontrol of chaos in continuous-time systems via time-delayed feedback, *Chaos*, Vol. 10(4), pp. 771-779, 2000.

[10] G. Chen and X. Dong, *From chaos to order : methodologies, perspectives and applications*, World Scientific, Singapore (1998).

[11] G. L. Baker, *American Journal of Physics*, vol. 63, pp. 832, 1995.

[12] W. L. Ditto, S. N. Rauseo, M.L. Spano, *Physical Review Letters*, vol. 65, pp. 3211, 1990.

[13] E. R. Hunt, *Physical Review Letters*, vol. 67, pp. 1953, 1991.

[14] J. Starrett, R. Tagg, *Physical Review Letters*, vol. 74, pp. 1974, 1995.

[15] S. J. Schiff *et al.*, *Nature*, vol. 370, pp. 615, 1994.

[16] R. Roy *et al.*, *Physical Review Letters*, vol. 68, pp. 1259, 1992.

[17] M. A. Matías, J. Güémez, *Physical Review Letters*, vol. 72, pp. 1455, 1994.

[18] J.M. Gutiérrez, A. Iglesias, J. Güémez, and M. A. Matías, *Int. Jour. of Bifurcation and Chaos*, vol. 6(5), pp. 1351, 1996.

[19] L.O. Chua, M. Komuro, T. Matsumoto "The double scroll family," *IEEE Trans. Circuits and Systems* vol. 33, 1073-1118, 1986.

[20] R. N. Madan, *Chua's Circuit: a paradigm for chaos*, World Scientific, Singapore (1993).

[21] A.lI. Khibnik, D. Roose, and L.O. Chua, *Int. Jour. of Bifurcation and Chaos,* vol. 3(2), pp. 363, 1993.

[22] G. P. King, S. T. Gaito, *Physical Review A* vol. 46, pp. 3092, 1992.

[23] G.-Q. Zhong, Memorandum No. UCB/ERL M94/42, UC Berkeley, 1994.

[24] K. Murali, M. Lakshmanan, *Physical Review E* vol. 48, pp. 1624, 1993.

Figure Captions

Figure 1. (a) Schematic of the cubic Chua's circuit consisting of three energy storage elements, one inductor and two capacitors, in parallel with a nonlinear resistance. The parameters have the following meaning: C_1 and C_2 are the two capacitances, L is the inductance, R is the resistance that couples the two capacitors and $R_{\rm L}$ is the inner resistance of the inductor. The variables that describe the dynamical system are v_1, v_2 and $i_{\rm L}$, the voltages across C_1 and C_2 and the current through L, respectively. (b) PSpiceAD analog simulation of the cubic polynomial $i - v$ characteristic of the nonlinear resistor.

Figure 2. Circuit implementation of the control device. The signal voltage sampled at point p is amplified in (A); then, it is converted to an intensity signal in the voltage-intensity conversor (VIC) and reinjected in p. The sampling process is controlled by the clock (C), and the switch (s) determines the positive or negative character of the pulses.

Figure 3. Time evolution in analog and numerical simulation. (a) Numerical simulation of system (2) with control (4) applied to variable y in the same conditions as the above analog simulation: $N = 2000$, $n = 10$ $\lambda = -0.15$; the numerical integration is carried out with a fourth order Runge-Kutta with integration steep $\tau = 2.5 \times 10^{-4}$ ($\approx 20\mu{\rm s}/N$). (b) Time evolution for capacitor voltages v_1 and v_2 in analog PSpiceAD simulation; the pulses are applied to v_2. (c) detail of a pulse: The interval of time between pulses is 20 μs and the pulse acts during 100 ns; after the pulse, variable v_2 varies in $\lambda \approx -91.38/620.48 \approx -0.15$.

Figure 4. Phase space and time evolution in oscilloscope view: (a) Phase space diagram for v_1 and v_2 in a double-scroll chaotic regime. (b) Temporal evolution of the controlled voltage v_2 on capacitor C_2 showing how the smooth evolution is periodically interrupted by pulses every $\tau = 20\mu$s; the sampled signal values taken to introduce the pulses are also shown. One of these pulses is magnified in the upper panel; after the pulse the voltage decays in $\lambda = -130/850 \approx -0.15$. (c) The stabilized period-2 orbit. (d) and (e) are similar to (b) and (d), but the pulses are applied every $\tau' = 10\mu$s. In this case, the voltage decays $\lambda' = -70/830 \approx -0.077$, verifying $\tau/\lambda = \tau'/\lambda'$.

Figure 5. (a) Bifurcation diagram for system (2) with α as bifurcation parameter. After a transient period, the maximum and minimum values $\overline{x}$ of the temporal evolution of variable $x \equiv v_1$ are represented. The numerical integration is carried out with a fourth order Runge-Kutta with integration step $\tau = 2.5 \times 10^{-3}$. (b) Bifurcation diagram associated with the control parameter λ for system (2) with control (4). The

circuit parameter values are $\alpha = 10$, $\beta = 13.06$, $\gamma = 0.00792$, $a = -1.089$, $b = 0.0033$; the control parameters in (4) are $N = 1000$ and $n = 10$. The control acts on variable $y \equiv v_2$; after a transient time, the maximum and minimum values of the temporal evolution of variable $x \equiv v_1$ are represented.

Figure 6. Osilloscope views of a sequence of stabilized circuit states obtained applying the control algorithm with decreasing λ values to the double scroll Chua's circuit shown in (a): (b) an orbit in a periodic window, (c) a single-scroll chaotic orbit, (d) a period four orbit, (e) a period two and (f) period one. The interval of time between pulses is 10 μs and the pulse acts during 100 ns.

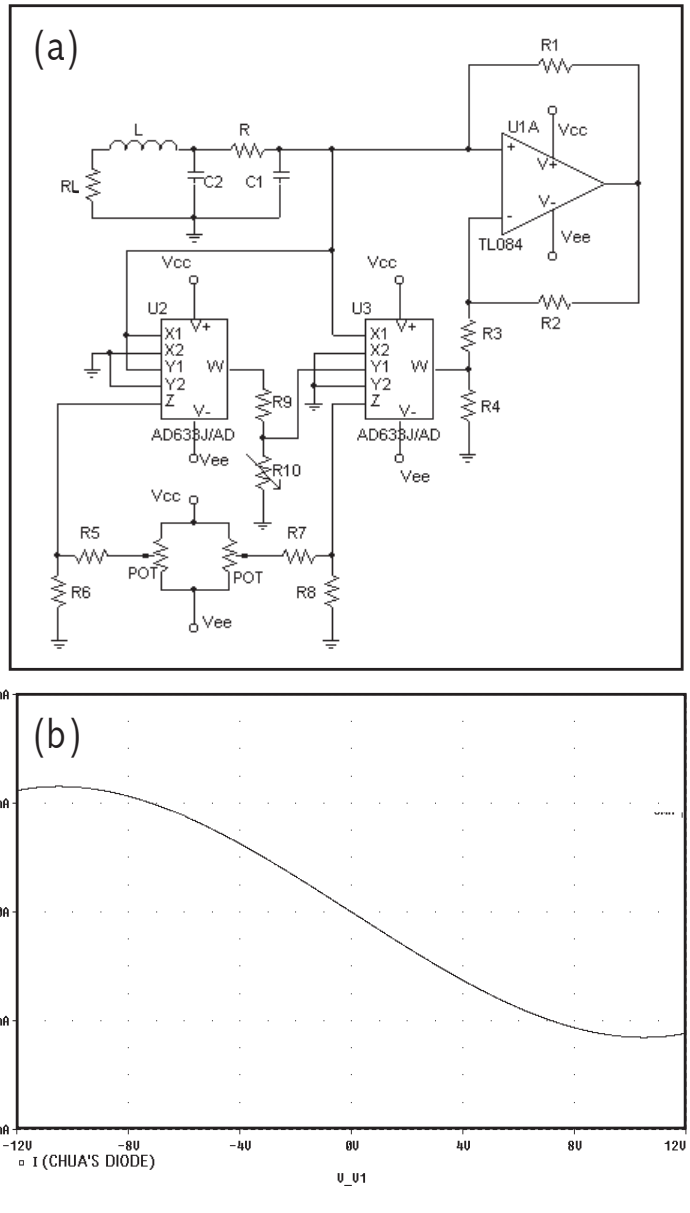

(a)
R1
L
R
RL
C2
C1
U1A
Vcc
V+
V-
Vee
TL084
Vcc
Vcc
U2
U3
X1
X2
Y1
Y2
Z
W
V+
V-
AD633J/AD
Vee
R3
R4
R2
R9
R10
Vcc
R5
R7
POT
POT
R6
R8
Vee
(b)
4.0mA
2.0mA
0A
-2.0mA
-4.0mA
-12V
-8V
-4V
0V
4V
8V
12V
I (CHUA'S DIODE)
V_V1

Figure 1

-

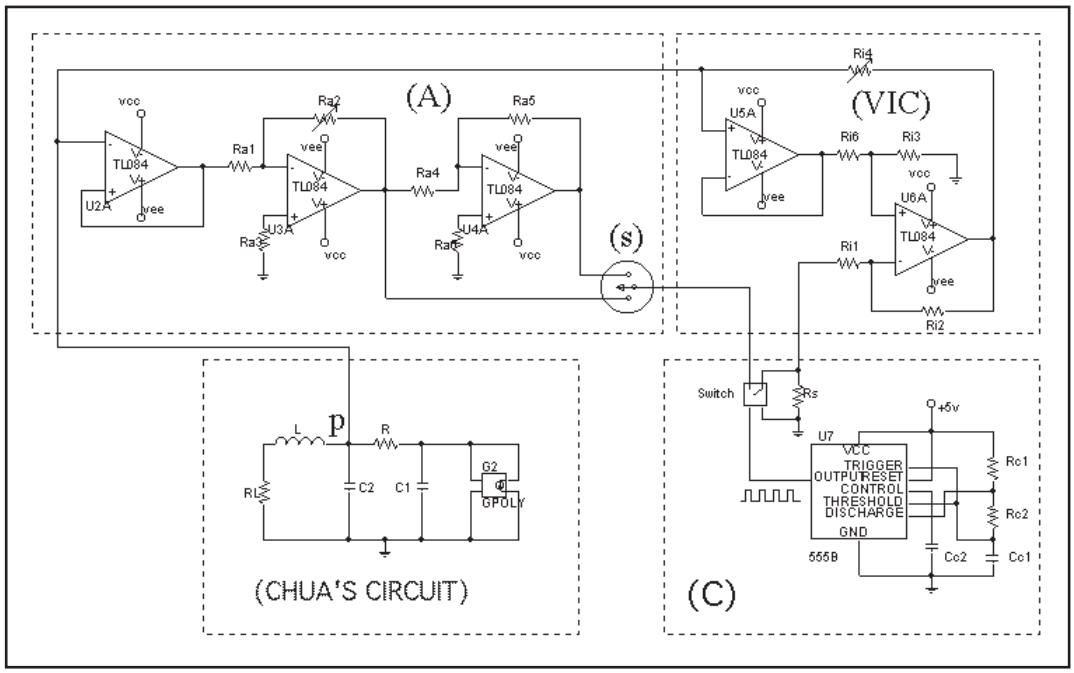

(A)
(VIC)
(s)
(CHUA'S CIRCUIT)
(C)
TL084
U2A
U3A
U4A
U5A
U6A
U7
vcc
vee
Ra1
Ra2
Ra3
Ra4
Ra5
Ra6
Ri1
Ri2
Ri3
Ri4
Ri6
Switch
Rs
+5v
555B
VCC
TRIGGER
OUTPUT
RESET
CONTROL
THRESHOLD
DISCHARGE
GND
Rc1
Rc2
Cc1
Cc2
L
R
p
RL
C1
C2
G2
GPOLY

Figure 2

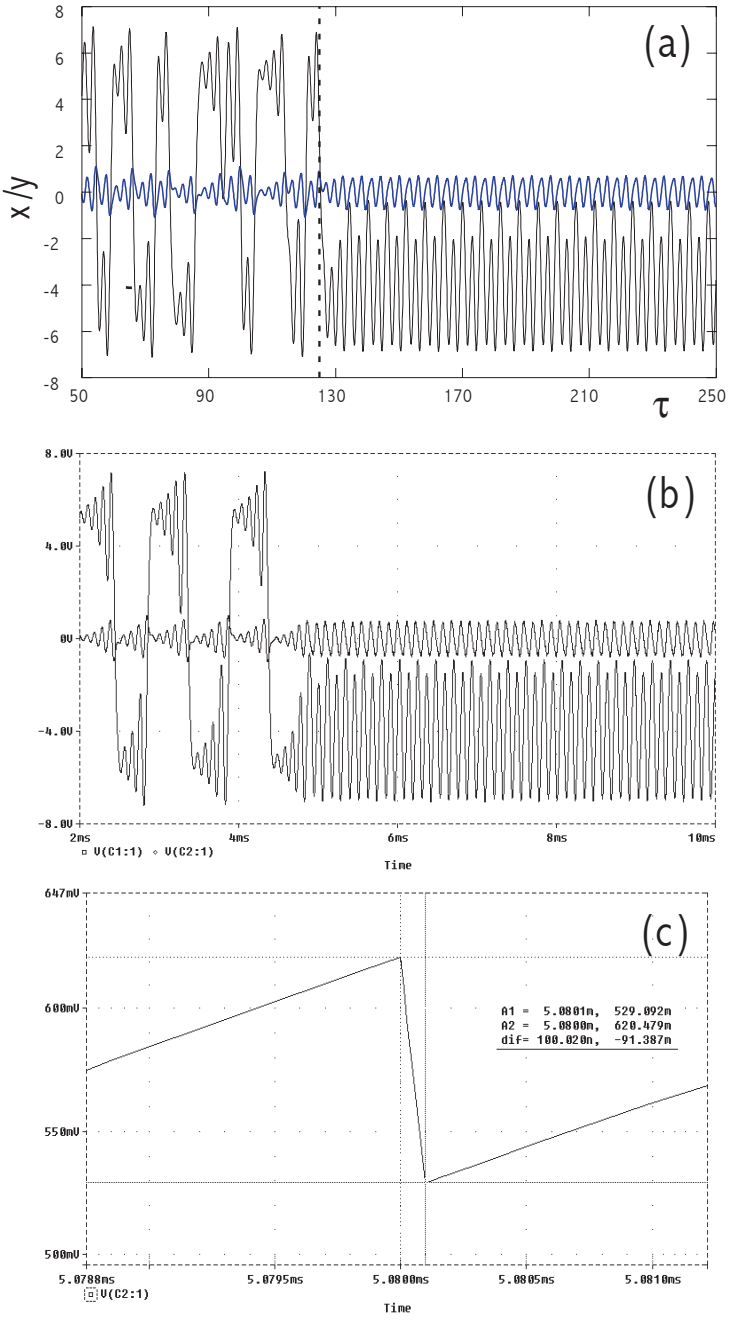

(a)
x /y
τ
(b)
V(C1:1)
V(C2:1)
Time
(c)
A1 = 5.0801m, 529.092m
A2 = 5.0800m, 620.479m
dif= 100.020n, -91.387m
V(C2:1)
Time

Figure 3

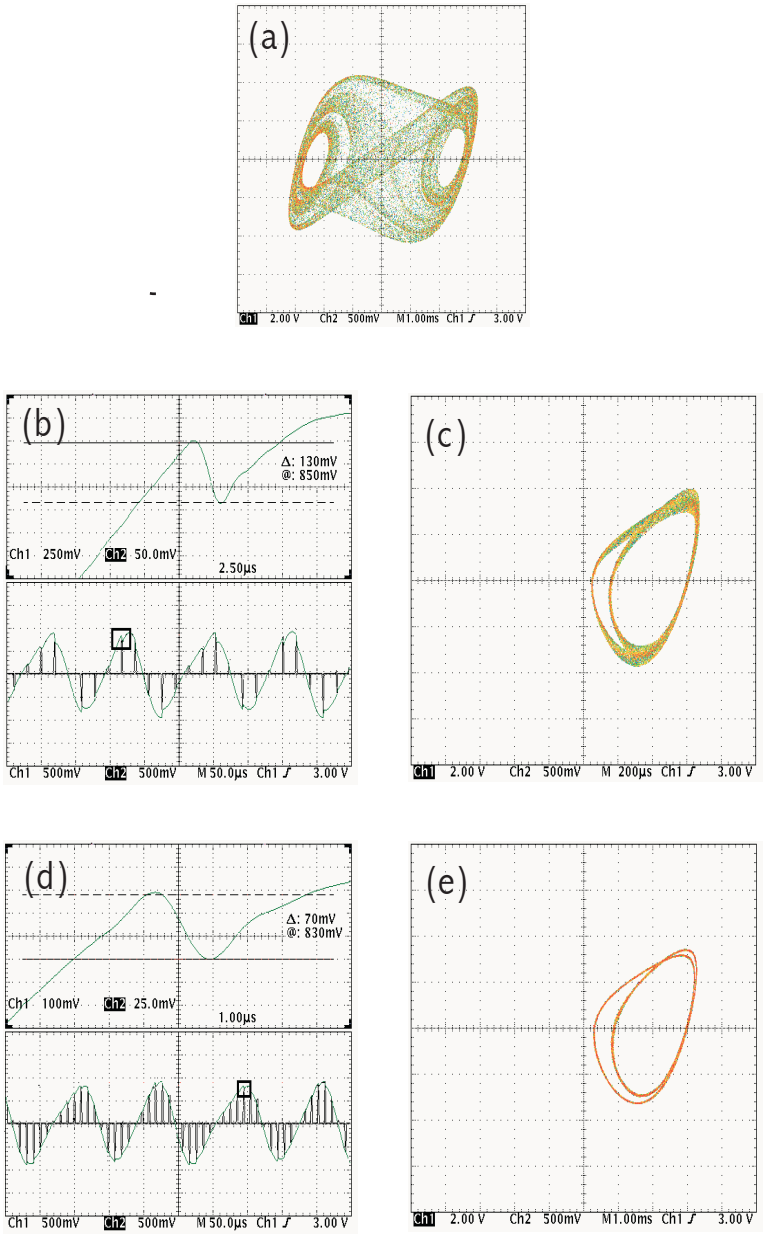

(a)
Ch1 2.00 V Ch2 500mV M1.00ms Ch1 ƒ 3.00 V
(b)
Δ: 130mV
@: 850mV
Ch1 250mV Ch2 50.0mV
2.50µs
Ch1 500mV Ch2 500mV M 50.0µs Ch1 ƒ 3.00 V
(c)
Ch1 2.00 V Ch2 500mV M 200µs Ch1 ƒ 3.00 V
(d)
Δ: 70mV
@: 830mV
Ch1 100mV Ch2 25.0mV
1.00µs
Ch1 500mV Ch2 500mV M 50.0µs Ch1 ƒ 3.00 V
(e)
Ch1 2.00 V Ch2 500mV M1.00ms Ch1 ƒ 3.00 V

Figure 4

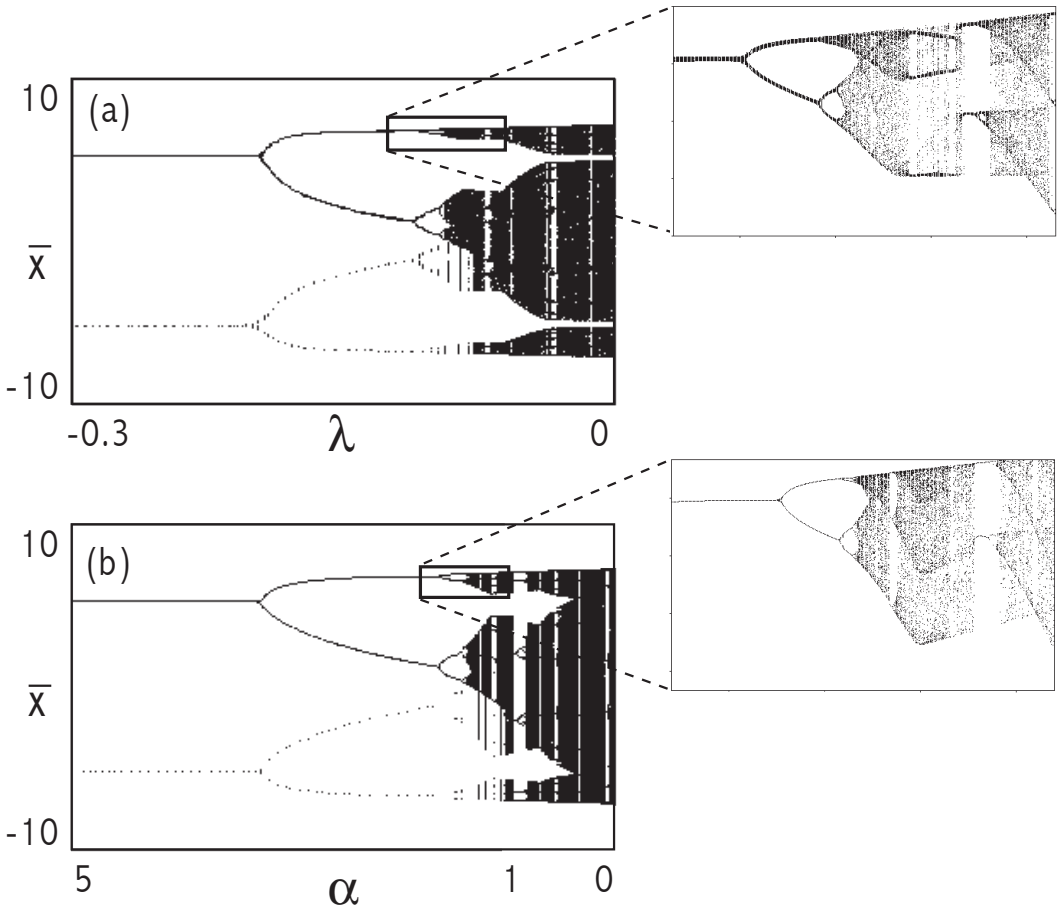


Figure 5

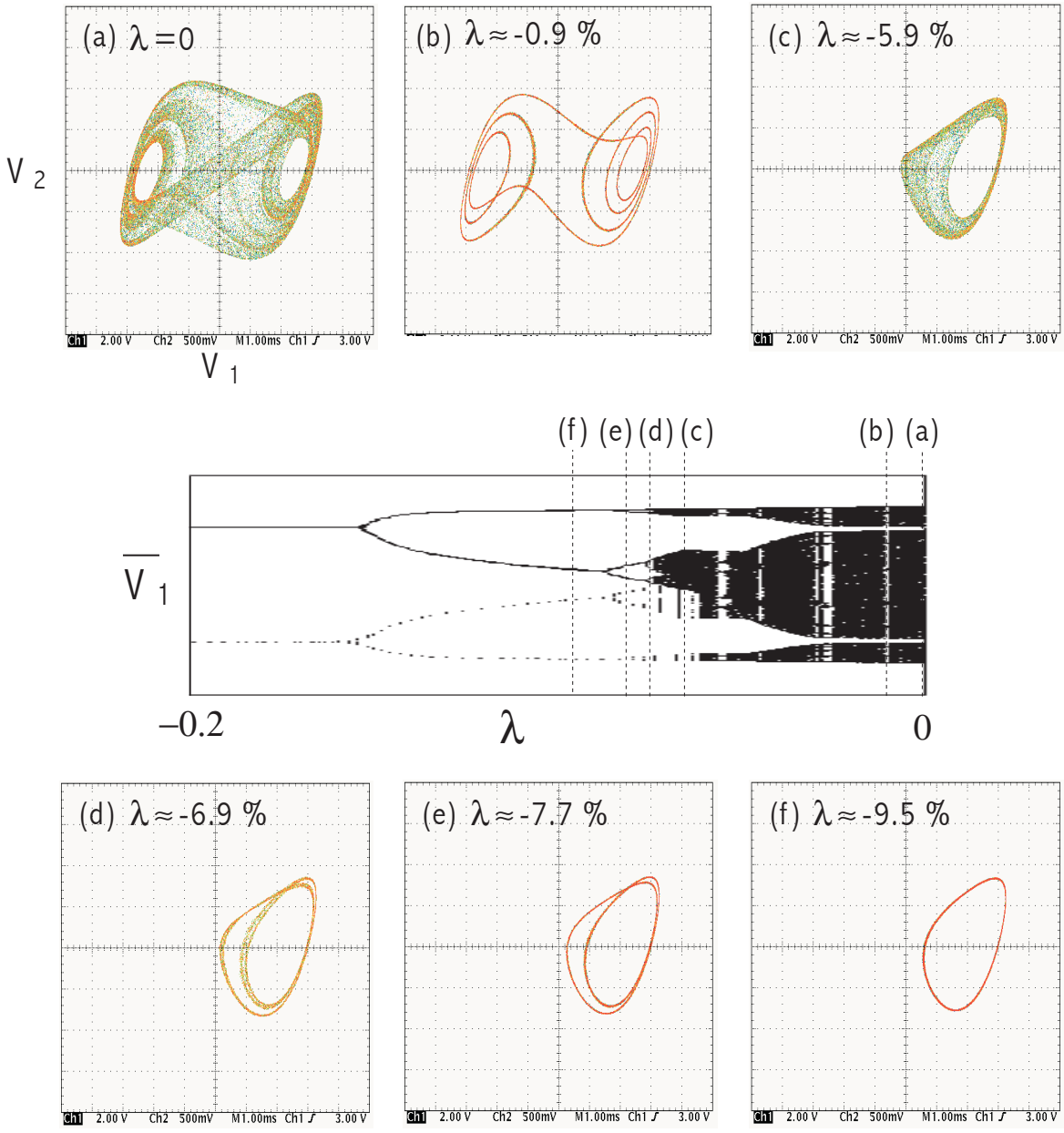


Figure 6